Resubmitted for consideration to Physical Review Letters

Directional-Dependent Thickness and Bending Rigidity of Phosphorene

Deepti Verma[1], Benjamin Hourahine[2], Thomas Frauenheim[3], Richard D. James[4], and Traian Dumitrică[1,5]

[1]*Department of Chemical Engineering and Materials Science, University of Minnesota, Minneapolis, MN 55455,U.S.A*

[2]*Department of Physics, SUPA, University of Strathclyde, Glasgow G4 0NG, United Kingdom*

[3]*Bremen Center for Computational Materials Science, University of Bremen, 28359 Bremen, Germany*

[4]*Department of Aerospace Engineering and Mechanics, University of Minnesota, Minneapolis, MN 55455,U.S.A*

[5]*Department of Mechanical Engineering, University of Minnesota, Minneapolis, MN 55455, U.S.A*

(Dated: June 20, 2016)

Abstract

The strong mechanical anisotropy of phosphorene combined with the atomic-scale thickness challenges the commonly employed elastic continuum idealizations. Using objective boundary conditions and a density functional-based potential, we directly uncover the flexibility of individual α, β and γ phosphorene allotrope layers along an arbitrary bending direction. A correlation analysis with the in-plane elasticity finds that although a monolayer thickness cannot be defined in the classical continuum sense, an unusual orthotropic plate with a directional-dependent thickness can unambiguously describe the out-of-plane deformation of α and γ allotropes. Such decoupling of the in-plane and out-of-plane nanomechanics might be generic for two-dimensional materials beyond graphene.

Phosphorene (PE) [1–3] — the crystalline two-dimensional (2D) material exfoliated from black phosphorous (BP) [4] — is attracting tremendous interest due to its exceptional electrical attributes, which include a high hole mobility (∼1,000 cm^2/Vs) [1], and its unique anisotropic in-plane mechanical, optical and thermal properties [5–13]. If strain is introduced in PE, further tuning of its exceptional properties can be achieved [14–17]. In practice, uniform strains could be applied by preparation of PE on flexible substrates [18]. Furthermore, the atomic-scale thickness should allow PE to conform to nearly any substrate [19, 20]. Thus, non-uniform strains could be induced by placing PE on nanoscale patterns and on nanoparticles [21, 22], or by pinning the 2D layer onto a substrate [23].

A key challenge for achieving strain engineering of PE is understanding its bending rigidity (D). As layers are approaching atomic-scale dimensions, deviations from continuum mechanics are expected [19, 24]. Thus, knowledge of the more accessible in-plane elasticity of PE does not warrant access to its out-of-plane deformation. Elastic theory requires defining a plate thickness (h). For PE, h is commonly assumed [6] to be 5.5 Å equilibrium interlayer distance in BP. However, it is not known if the selection of this h leads to consistency between the axial and bending moduli of PE. In graphene — the one-atom thick layer exhibiting only surfaces — there is a decoupling of the bending from the tensional deformations [19, 25]. To fit the isotropic plate, a sub-atomic thickness rather than the inter-layer spacing of graphite should be selected [19, 26].

In this Letter we use PE allotropes as model systems to study the applicability of the classical plate elasticity to few-atom-thick 2D layers. The investigated structures are displayed in Figs. 1a-c: (i) In α PE, Fig. 1a, the P atoms are disposed in a honeycomb lattice that is periodically rippled with a sub-nanometer periodicity. It presents two type of P-P bonds: "surface" bonds oriented nearly along the **a**+**b** direction, where **a** and **b** are the unit lattice vectors, and "internal" bonds connecting P atoms located on the two surfaces. (ii) β PE [27], Fig. 1b, contains only "internal" bonds, as the P atoms of the honeycomb lattice are only buckled up and down in an alternating manner. (iii) γ PE [28], Fig. 1c, presents both "surface" bonds (oriented along the **b** direction) and "internal" bonds. We show via atomistic calculations and continuum analysis that the bending of PE deviates from the classical plate mechanics, and that this deviation is reflected into a thin plate model with directional-dependent h. This model is able to capture the nanomechanics of bending and in-plane stretching, such as for example when stretching of the layer reduces

the effective curvature via the Poisson effect.

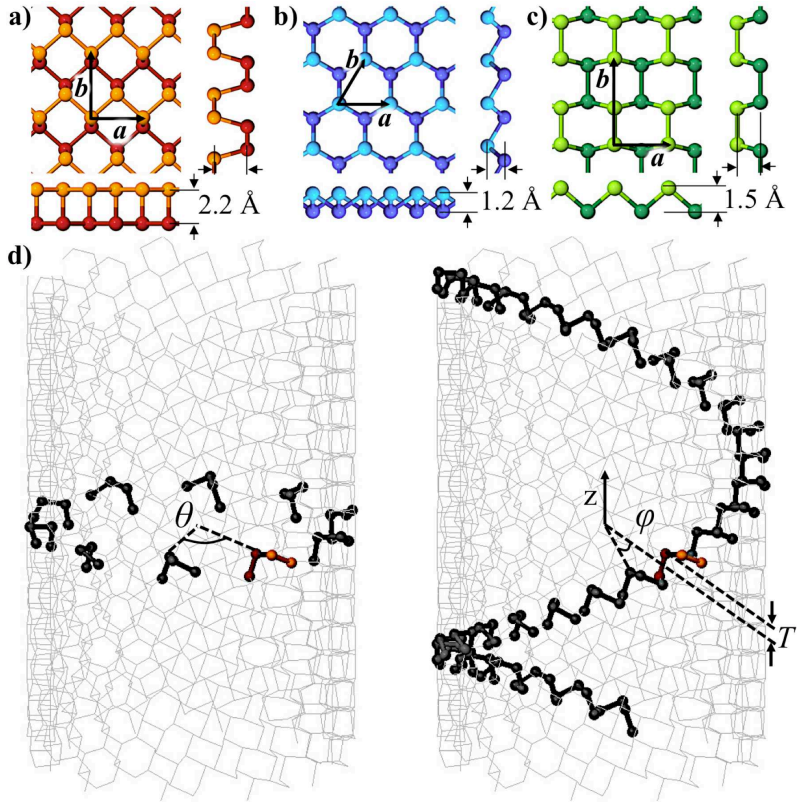

FIG. 1: Top, side views, and lattice vectors (**a**, **b**) of a) α PE ($a = 3.49$ Å, $b = 4.35$ Å), b) β PE ($a = b = 3.68$ Å), and c) γ PE ($a = 3.45$ Å, $b = 5.54$ Å). To guide the eye, the atoms and bonds located on the two surfaces are displayed in different shades. The layer thickness is also shown. d) A (10,20) α NT is represented by applying to the 4 atom basis cell a finite number of rotations $\theta = 10°$ (left) and infinite number of rotations of angle $\varphi = 15.50°$ around the NT axis combined with translation $T = 1.62$ Å along the NT axis.

In order to quantify the energetics of PE bending, we have performed objective molecular dynamics (OMD) simulations [29] coupled with symmetry-adapted non-orthogonal tight-binding [30, 31]. We simulate a bent PE with curvature κ along a direction $\mathbf{C} = n\mathbf{a} + m\mathbf{b}$

as a (n,m) nanotube (NT) with radius $R = 1/\kappa$ and chirality χ, where χ is the angle made by $\mathbf{C}$ and $\mathbf{a}$. OMD is a simulation method based on the concept of objective structures [32]. The objective molecular structure description [30, 32] of NTs employed here writes

$$\mathbf{X}_{l,i,j} = i\mathbf{T} + \mathbf{R}_1^j \mathbf{R}_2^i \mathbf{X}_l, \quad l = 1, ..., N, \tag{1}$$

$$\mathbf{T} \equiv \begin{bmatrix} 0 \\ 0 \\ T \end{bmatrix}, \quad \mathbf{R}_\delta \equiv \begin{bmatrix} \cos\delta & -\sin\delta & 0 \\ \sin\delta & \cos\delta & 0 \\ 0 & 0 & 1 \end{bmatrix}.$$

In the above, $\mathbf{R}_1 = \mathbf{R}_\theta$, where θ is the angle describing the angular rotation, and $\mathbf{R}_2 = \mathbf{R}_\varphi$, where φ are the angle comprising the helical operation. T is the translation component of the helical operation. $\mathbf{X}_l$ are the Cartesian coordinates of one of the N atoms located in the unit cell, $\mathbf{X}_{l,i,j}$ are the coordinates of the i-th helical and j-th angular image of this atom. As an example, Fig. 1a shows how an infinite α NT is built out of a unit cell containing $N = 4$ atoms. Similarly, β and γ PE NTs can be built from the $N = 2$ and $N = 4$ atom basis, respectively. With OMD, any PE NT can be calculated by considering only the minimal basis of N atoms placed under the objective boundaries described by eq. (1).

Our calculations are carried out with a developmental version of the code DFTB+ [33]. We describe the interatomic interactions with a density functional theory-based (DFTB) potential [34] which comprises *spd* orbitals located on each P atom. The symmetry-adapted tight-binding formulation [30, 31] is compatible with eq. (1) as its incorporates helical and angular symmetries. Here, we simulated a collections of α, β, and γ NTs with radii 11 nm $< R <$ 75 nm. Conjugate-gradient relaxations were performed until the magnitude of the force on every atom was less than 10^{-6} Hartree/Bohr. The Brillouin zone in the helical direction was sampled with 20 k points. All allowed discrete k values in the pure rotational direction [30] were calculated.

The rolled-up construction [35] of Kirchhoff's plate theory [36] describes an exact isometric mapping of the PE sheets shown in Fig. 1a-c. Due to finite curvature effects, the bond lengths and bond angles will be changed upon rolling. If significant, these changes will reflect in a departure from the ideal values of the structural parameters φ and T. Nevertheless, in our simulations we have found that at large radii, the NT structures with ideal φ and T helical parameters [35] correspond directly to local minima of the potential energy (U). As exemplified in Figs. 2a and b for the case of a (800,0) α NT, the variations (one

at a time) of the translation T and rotation angles φ around the ideal values [35] lead to energy increase. During the structural relaxations, the N atoms are free to move along the radial NT direction. After relaxation, each NT radius was measured as the average radius described by the simulated atoms. Fig. 2c shows that while NTs expand to radii slightly larger than those predicted by the roll-up construction, the measured radial pre-strain ϵ_R is negligible. This means that the circumference of the (n,m) NT equals the length of the original 2D vector $\mathbf{C}$.

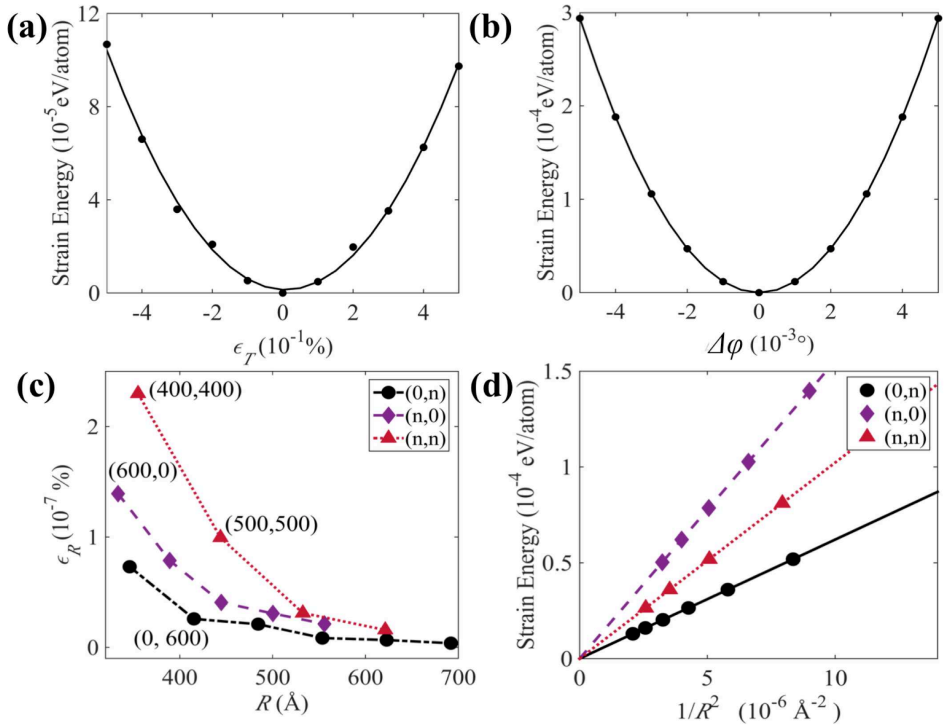

FIG. 2: a) Strain energy of (800,0) α NT as the translation T and b) angle φ are varied around the values predicted by the roll-up construction. Here $\epsilon_T = \Delta T/T$. c) Radial prestrain, $\epsilon_R = \Delta R/R$, vs. the ideal of α NT radius R. d) Strain energy of α NTs vs. curvature squared, with fitted linear curves.

Because the OMD calculations revealed that deviations from the roll-up construction are negligible, we can conclude that large-diameter NTs store only bending energy. Thus, the slopes of the lines of Fig. 2d correspond to D^α with reference to α PE. Table 1 summarizes the obtained $D = (1/|\mathbf{a} \times \mathbf{b}|)\partial^2 U/\partial^2 \kappa$ along the lattice vector directions. We find that D in the $\mathbf{a}$ and $\mathbf{b}$ directions are essentially identical for β PE, but very different for α and γ

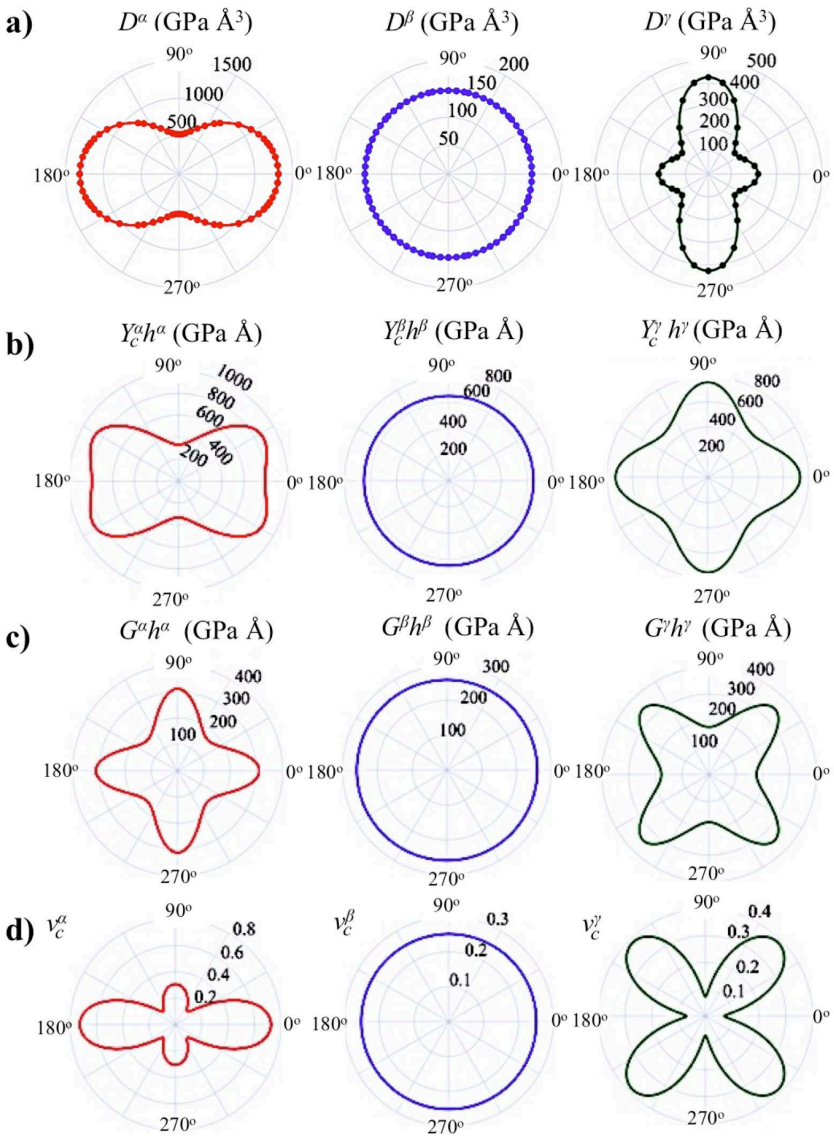

FIG. 3: a) Bending moduli of α (left), β (center) and γ (right) PE as a function of direction. Data points are the DFTB OMD calculations. b) In-plane stretching stiffness, c) shear stiffness, and d) Poisson's ratios as a function of direction.

PEs. For example, D^{α} along the zig-zag direction is ~ 2.5 larger that along the armchair direction. Interestingly, the most stable allotrope α presents D^{α} values significantly larger than D^{β} and D^{γ}.

Fig. 3a gives the D dependence on χ. The fitting of the computed data leads to the

interpolations

$$D^{\alpha}/\text{GPa Å}^3 = 934 + 393\cos 2\chi - 16\cos 4\chi, \tag{2a}$$

$$D^{\gamma}/\text{GPa Å}^3 = 243 - 104\cos 2\chi + 79\cos 4\chi. \tag{2b}$$

From the earlier studies of small-diameter carbon NTs, it is known that curvature can alter the carbon-carbon bonding [25] to the extent that the elastic constants will show χ dependence and will differ from those of graphene [37, 38]. We emphasize that the results reported here for PE are carried out in a regime in which there is no significant change in P-P bonding under finite κ. To further confirm this point we have compared the in-plane elastic properties of the NT wall with those computed for the flat lattice, which are summarized in Table 1. Our comparison focused on the deformations along the preferential **a** and **b** directions, where energy scans revealed that the NT elongation and twist deformations are uncoupled. For example, the parabolic energy dependences of Figs. 2a and b are pure stretching and shear energies, respectively. The resulting stretch and shear stiffness values of 337 GPa Å and 311 GPa Å, respectively, are very close to the corresponding $Y_b h$ and Gh of the flat layer (Table 1). Thus, the $D(\chi)$-dependence reported here is due to the manner in which the P atoms are bonded in the different allotrope layers the P-P bonding and not to the significant curvature.

TABLE I: The principal bending moduli, in-plane stiffness and Poisson's ratios of α, β, and γ PEs, as obtained from the DFTB model [34]. In α and γ PEs, subscript a and b correspond to the zig-zag and armchair directions, respectively.

	D_a	D_b	$Y_a h$	$Y_b h$	$G_a h$	ν_a	ν_b
	GPa Å^3	GPa Å^3	GPa Å	GPa Å	GPa Å		
α:	1,311	524	791	333	312	0.73	0.31
β:	147	147	649	649	259	0.25	0.25
γ:	219	426	734	755	178	0.07	0.07

While β PE is isotropic, α and γ PEs present orthotropic symmetry with **a** and **b** being the principal directions. An orthotropic plate requires four independent elastic moduli, i.e.,

the Young's moduli Y_a and Y_b, the shear modulus G, and the Poisson's ratio ν_a. (Note that $\nu_b = \nu_a Y_b/Y_a$). For a broader view, Table 1 summarizes our elastic moduli calculations for the flat α, β, and γ PEs. We note that the PE Young's moduli are overall an order of magnitude lower that graphene's 4,300 GPa Å value [25, 40]. Nevertheless, α PE is less flexible than graphene, which has a bending modulus of only 230 GPa Å^3 [19].

In general, a plain stress (σ_c) applied along the **C** direction of an orthotropic plate leads not only to layer extension (ε_c) along **C** and layer compression along the perpendicular direction **T** (ε_t), but also to a shear deformation (ε_{ct}). The stress-strain relation writes [35]

$$\begin{pmatrix} \varepsilon_c \\ \varepsilon_t \\ \varepsilon_{ct} \end{pmatrix} = \begin{bmatrix} \frac{1}{Y_c h} & \frac{-\nu_t}{Y_t h} & \frac{\eta_c}{Gh} \\ \frac{-\nu_c}{Y_c h} & \frac{1}{Y_t h} & \frac{\eta_t}{Gh} \\ \frac{\eta_c}{Gh} & \frac{\eta_t}{Gh} & \frac{1}{Gh} \end{bmatrix} \begin{pmatrix} \sigma_c h \\ \sigma_t h \\ \sigma_{ct} h \end{pmatrix}. \tag{3}$$

The shear-strain coupling coefficients η_c and η_t vanish when $\chi = 0$ or 90° [35]. The stretching stiffness ($Y_c h$ and $Y_t h$), shear (Gh) stiffness, and Poisson's ratios (ν_c and ν_t) relate to the surface elastic constants along the principal axes (Table 1) via closed form expressions [35]. Plots from these standard equations for the elastic constant along **C** are shown in Fig. 3b-d. The plots for the stretching stiffness along **T** are 90° rotated with respect to those shown in Fig. 3b, i.e. $Y_c h(\chi) = Y_t h(\chi + 90°)$ [35].

Eq. (3) makes it transparent that h is not needed in order to describe the in-plane deformation of PE. Defining h is nevertheless required in order to correlate the in-plane elasticity with the out-of-plane bending deformations. To find h, we equate the bending rigidity of the plate with the D found by direct OMD calculations, as

$$\frac{Y_c h^3}{12(1-\nu_t \nu_c)} = D. \tag{4}$$

The obtained h, displayed in Fig. 4a, are different from the interlayer spacing in BP. They are physically meaningful, in the sense that the h values are not sub-atomic. The thickness of β PE, $h = 1.6$ Å, is uniform. For α and γ PEs, h is χ-dependent, as

$$h^\alpha/\text{Å} = 3.8 - 0.5\cos 2\chi - 0.2\cos 4\chi, \tag{5a}$$

$$h^\gamma/\text{Å} = 2.1 - 0.4\cos 2\chi + 0.2\cos 4\chi. \tag{5b}$$

Thus, the differences in atomic bonding between α and γ are playing an important role in defining h. We note in passing that while a κ-dependent orthotropic shell was proposed as

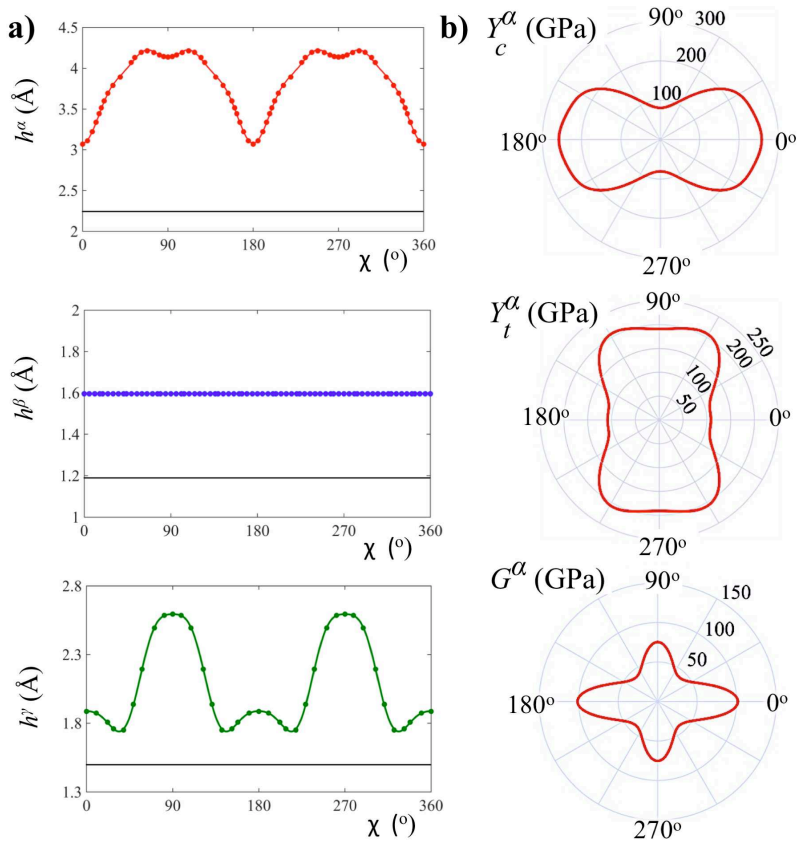

FIG. 4: a) χ-dependence of h for α, β and γ PE. The black continuous line is h measured from the atomic positions, Fig. 1a-c. b) χ-dependence of the circumferential and axial Young's moduli and of the shear modulus, for α PE.

the equivalent representation of chiral NTs [37], this is the first time when a χ-dependent plate model is being developed to model 2D materials. To reach large curvatures (not considered here), the current model should develop an additional κ-dependence.

We emphasize that given a bending direction χ, the proposed orthotropic plate models for α and γ PEs still rely on four independent constants. The selection of the elastic constants requires care, as the $h(\chi)$ dependence paradox leads to $Y_c(\chi) \neq Y_t(\chi + 90°)$. For example, Fig. 4b plots the Y_t, Y_c, G obtained by dividing by $h(\chi)$ the surface value discussed before

for α PE. It can be seen that Y_t and Y_c for α PE are not related by a 90° rotation, and that $G_a \neq G_b$. Nevertheless, the orthotropic model is functional as long as Y_t, Y_c, G at a particular χ are selected from the three separate graphs shown in Fig. 4b.

The impossibility of fitting our data by a unique h reflects the differences between the classical continuum and the underlying molecular mechanics description. Indeed, the classical plate model assumes that the bending strain originates in the extension (compression) of the continuum material above (under) the mid-plane. In PE, the bending strain is stored in small bond length and angle changes upon roll-up, captured here by the changes in the quantum interatomic matrix elements and repulsive potential [34]. A compelling example for the decoupling between bending and in-plane stretching is provided by the χ-dependence of D^γ and $Y^\gamma h$ plotted in Figs. 3a and b. Along the principal directions, γ PE presents similar resistance to stretching. However, it is twice as hard to bend along the **b** direction than in the perpendicular **a** direction. In the former case, the roll-up mapping gives stretching and compression of the surface P-P bonds, Fig. 1c. In the latter, the length of the surface bonds remain unchanged; finite curvature is accommodated through bond length and angle changes involving bonds connecting P atoms on the two surfaces. Although h measured from the atomic positions is unique, χ-dependence of h is needed in order to correlate the nanomechanics of bending and in-plane stretching. Interestingly, the $h(\chi)$ paradox leads to the in-plane stretching contradiction captured by Fig. 4b.

Understanding how the mechanical behavior of materials deviates at the nanoscale from the macroscopically established concepts [36] is an outstanding problem. Here we show that in PE, this deviation is manifested in the χ-dependent h paradox. Nevertheless, the developed orthotropic plate model is unambiguous. It can be broadly useful for developing the strain- and ripple-[41] engineering of PE, and for designing PE kirigami [42]. More broadly, the decoupling of in-plane and out-of-plane deformations identified here for PE is likely generic to 2D structures made from layered or non-layered materials. This finding has important implications for the future development of continuum idealization of 2D structures as the commonly-accepted continuum models developed for bulk need to be adapted for structures with atomic-scale thicknesses. The OMD calculations based on DFTB potentials offer a robust way to predict the bending response needed to establish these continuum idealizations.

Computations were carried out at the Minnesota Supercomputing Institute.

[1] L. Li, Y. Yu, G. J. Ye, Q. Ge, X. Ou, H. Wu, D. Feng, X. H. Chen, and Y. Zhang, *Nat. Nanotechnol.* **9**, 372 (2014).

[2] H. Liu, A. T. Neal, Z. Zhu, Z. Luo, X. Xu, D. Tománek, and P. D. Ye, *ACS Nano* **8**, 4033 (2014).

[3] P. Yasaei, B. Kumar, T. Foroozan, C. Wang, M. Asadi, D. Tuschel, J. E. Indacochea, R. F. Klie, and A. Salehi-Khojin, *Adv. Mater.* **27**, 1887 (2015).

[4] P. W. Bridgman, *J. Am. Chem. Soc.* **36** , 1344 (1914).

[5] S. Appalakondaiah, G. Vaitheeswaran, S. Lebégue, N. E. Christensen, and A. Svane, *Phys. Rev. B* **86**, 035105 (2012).

[6] Q. Wei and X. Peng, *Appl. Phys. Lett.* **104**, 251915 (2014).

[7] J. Tao, W. Shen, S. Wu, L. Liu, Z. Feng, C. Wang, C. Hu, P. Yao, H. Zhang, W. Pang, X. Duan, J. Liu, C. Zhou, and D. Zhang, *ACS Nano* **9**, 11362 (2015).

[8] R. Fei and L. Yang, *Nano Lett.* **14**, 2884 (2014).

[9] Z. Wang and P. X.-L. Feng, *2D Mater.* **2**, 021001 (2015).

[10] X. Wang, A. M. Jones, K. L. Seyler, V. Tran, Y. Jia, H. Zhao, H. Wang, L. Yang, X. Xu, and F. Xia, *Nature Nanotechnol.* **10**, 517 (2015).

[11] H. Jang, J.D. Wood, C.R. Ryder, M.C. Hersam, and D.G. Cahill, *Adv. Mater.* **27**, 8017 (2015).

[12] Z. Luo, J. Maassen, Y. Deng, Y. Du, R. P. Garrelts, M. S. Lundstrom, P. D. Ye, and X. Xu, *Nature Commun.* **6**, 8572 (2015).

[13] A. Chaves, T. Low, P. Avouris, D. Cakir, and F. M. Peeters, *Phys. Rev. B* **91**, 155311 (2015).

[14] M. Mehboudia, K. Utta, H. Terrones, E. O. Harriss, A. A. P. SanJuan, and S. Barraza-Lopeza, *Proc. Natl. Acad. Sci. USA* **112**, 5888 (2015).

[15] A.S. Rodin, A. Carvalho, and A.H. Castro Neto, *Phys. Rev. Lett.* **112**, 176801 (2014).

[16] D. Akinwande, N. Petrone, and J. Hone, *Nat. Commun.* **5**, 5678 (2014).

[17] Z. Chen, G. Huang, I. Trase, X. Han, and Y. Mei, *Phys. Rev. Appl.* **5**, 017001 (2016).

[18] X. Li, B. Deng, X. Wang, S. Chen, M. Vaisman, S. Karato, G. Pan, M.L. Lee, J. Cha, and H. Wang, *2D Mater.* **2**, 031002 (2015).

[19] D.-B. Zhang, A. Akatyeva, and T. Dumitrică, *Phys. Rev. Lett.* **106**, 255503 (2011).

[20] J.S. Bunch and M.L. Dunn. *Solid State Commun.* **152**, 1359 (2012).

[21] M. Yamamoto, O. Pierre-Louis, J. Huang, M. S. Fuhrer, T. L. Einstein, and W. G. Cullen. *Phys. Rev. X* **2**, 041018 (2012).

[22] E. Monazami, L. Bignardi, P. Rudolf, and P. Reinke, *Nano Lett.* **15**, 7421 (2015).

[23] F. Wang, G. Liu, S. Rothwell, M. Nevius, A. Tajeda, A. Taleb-Ibrahimi, L.C. Feldman, P.I. Cohen, and E.H. Conrad, *Nano Lett.* **13**, 4827 (2013).

[24] Y. Zheng, J. Chen, M.-F. Ng, H. Xu, Y.P. Liu, A. Li, S.J. O'Shea, T. Dumitrică, and K.P. Loh, *Phys. Rev. Lett.* **114**, 065501 (2015).

[25] I. Nikiforov, E. Dontsova, R.D. James, T. Dumitrică, *Phys. Rev. B* **89**, 155437 (2014).

[26] S.S. Gupta, F.G. Bosco, and R.C. Batra. *Comp. Mat. Sci.* **47**, 1049 (2010).

[27] J.C. Jamieson, *Science* **39**, 1291 (1963).

[28] J. Guan, Z. Zhu and D. Tománek, *Phys. Rev. Lett.* **113**, 046804 (2014).

[29] T. Dumitrică and R. D. James, *J. Mech. Phys. Solids* **55**, 2206 (2007).

[30] D.-B. Zhang, M. Hua, and T. Dumitrică, *J. Chem. Phys.* **128**, 084104 (2008).

[31] I. Nikiforov, B. Hourahine, B. Aradi, Th. Frauenheim, and T. Dumitrică, *J. Chem. Phys.* **139**, 094110 (2013).

[32] R.D. James, *J. Mech. Phys. Solids* **54**, 2354 (2006).

[33] B. Aradi, B. Hourahine, and T. Frauenheim, *J. Phys. Chem. A* **111**, 5678 (2007).

[34] Y. Yang, H. Yu, D. York, M. Elstner, and Q. Cui, *J. Chem. Theory Comput.* **4**, 2067 (2008)

[35] See supporting information for the rolled-up construction of NTs, OMD calculations of chiral NTs, elastic constants for an orthotropic plate stressed in non-principal coordinates, and the χ-dependence of elastic constants.

[36] For the history see G. Frieseke, R. D. James, and S. Müller, *Comm. Pure Appl. Math.* **LV**, 146 (2002).

[37] L. Wang, Q. Zheng, J. Z. Liu, and Q. Jiang, *Phys. Rev. Lett.* **95**, 105501 (2005).

[38] D.B. Zhang and T. Dumitrică, *Appl. Phys. Lett.* bf 93, 031919 (2008).

[39] M. Wu, H. Fu, L. Zhou, K. Yao, and X. C. Zeng, *Nano Lett.* **15**, 3557 (2015).

[40] C. Lee, X. Wei, W. Kysar, and J. Hone, *Science* **321**, 385 (2008)

[41] M.C. Wang, S.G. Chun, R.S. Han, A. Ashraf, P. Kang, and S.W. Nam, *Nano Lett.* **15**, 1829 (2015).

[42] B.F. Grosso and E.J. Mele, *Phys. Rev. Lett.* **115**, 195501 (2015).